IEEE Access
Multidisciplinary : Rapid Review : Open Access Journal

Received May 1, 2018, accepted June 18, 2018, date of publication July 2, 2018, date of current version July 25, 2018.

Digital Object Identifier 10.1109/ACCESS.2018.2850902

Polarization-Angle-Frequency Estimation With Linear Nested Vector Sensors

XIAODONG HAN, TING SHU, JIN HE, AND WENXIAN YU
Shanghai Key Laboratory of Intelligent Sensing and Recognition, School of Electronic Information and Electrical Engineering, Shanghai Jiao Tong University, Shanghai 200240, China

Corresponding author: Ting Shu (tingshu@sjtu.edu.cn)

This work was supported in part by the National Natural Science Foundation of China under Grant 61771302, in part by the Scientific Research Plan of Shanghai Science and Technology Commission under Grant 16511103004, and in part by the Aeronautical Science Foundation of China under Grant 2015ZD07006.

ABSTRACT This paper considers the problem of multiple dimensional parameter estimation of radar signals using a linear nested vector sensor array. We propose a computationally efficient polarization-angle-frequency estimation algorithm based on spatial-temporal nested sampling. Radar cross-sections diversity in multiple coherent processing intervals is exploited to construct a virtual polarization-spatial-temporal manifold with extended degrees of freedom. Then, a computational efficient method without eigen-decomposition is derived to estimate Khatri-Rao signal subspace. Automatically paired polarization, azimuth-elevation angles, and doppler frequency estimates are finally obtained by exploiting the idea of the estimation of signal parameters via rotational invariance techniques algorithm. The effectiveness of the proposed method is verified through numerical examples.

INDEX TERMS Angle and frequency estimation, polarization estimation, pulsed Doppler, nested sampling, nested array, degree of freedom.

I. INTRODUCTION

THE problem of estimating multiple parameters (including angles, frequencies and polarization) of targets is very important in many application scenarios of radar array processing. Accurate estimation of angle and frequency parameters enables the better target localization and tracking performance, and precise polarization information extraction offers better target classification and recognition performance. During the past decade, many efficient multidimensional parameter estimation methods have been presented. These methods include azimuth-elevation angle estimation methods [1]–[4], joint angle and frequency estimation methods [5]–[9], and angle-polarization estimation methods [10]–[15].

Most of the radar array processing methods consider that the spatio-temporal data samples are taken uniformly with Nyquist rate, and consequently, have limited degree of freedom in both space and time domain. Recently, it is shown that measuring spatial data with nonuniform nested arrays can offer enhanced spatial degree of freedom for angle estimation [16]. Specially, spatial measurements with $\mathcal{O}(N)$ nested samples can provide $\mathcal{O}(N^2)$ degree of freedom, and therefore, enables the resolution of K signals with $N < K$ spatial samples. Data acquisition with spatially nested sampling has been found in solving various radar signal processing problems such as detection [17], localization [18], [19], and jamming suppression [20].

For multiple dimensional parameter estimation, nested sampling can be exploited in each dimension for use of Khatri-Rao (K-R) subspace-based parameter estimation methods with degree of freedom enhancement. For example, [21] develops a two-dimensional angle estimation method using L-shaped nested array; [22] considers nested sampling in spatial and time delay domains for angle and range estimation; and [23] proposes nested spatio-temporal sampling for joint angle and doppler frequency estimation. The algorithms in [21]–[23] achieve the the degree of freedom enhancement for parameter estimation, however, they have some drawbacks that limit their practical applications. Firstly, the estimation of two-dimensional angles requires the use of planar array geometries, which is unsuitable for some practical situations such as airborne application, where the physical space available for antenna deployment is very limited. Secondly, nested sampling enhances the degree of freedom, but also increases the computational costs involved in K-R subspace computation, and consequently, these methods are unsuitable for applications where the parameters of targets should be estimated promptly.

Therefore, the purpose of this paper is to investigate the multiple dimensional parameter estimation of radar signals in a geometrically and computationally simple manner. Motivated by the fact that linear vector antenna array can be used to estimate two-dimensional angles [24], we propose a polarization-angle-frequency estimation algorithm using a linear nested vector sensor array. Firstly, radar cross-sections (RCSs) diversity in multiple coherent processing intervals (CPIs) to is exploited to construct a virtual polarization-spatial-temporal (PST) manifold with extended degree of freedom. Then, a computational efficient method without eigen-decomposition is derived to estimate K-R signal subspace. Finally, automatically paired polarization, 2D angles and frequency estimates are obtained by using the idea of the estimation of signal parameters via rotational invariance techniques (ESPRIT) algorithm. Incidentally, the use of nested sampling can offer improved identification performance as well as parameter estimation performance. Moreover, radars transmit pulses non-uniformly can improve their performance for low probability of intercept (LPI).

Notation: Throughout the paper, scalar quantities are denoted by lowercase letters. Lowercase bold type faces are used for vectors and uppercase letters for matrices. Superscripts T, H and $*$ represent the transpose, conjugate transpose and complex conjugate, respectively, $\otimes$, $\odot$ and $\diamond$ symbolize the Kronecker product, Khatri-Rao (column-wise Kronecker) matrix product, and element-by-element multiplication, respectively, $\boldsymbol{I}_m$ denotes the $m \times m$ identity matrix, and $\boldsymbol{e}_n$ stands for a vector of all zeros except a 1 at the nth position.

II. PROBLEM FORMULATION

The present problem focuses on the estimation of angle, frequency and polarization parameters of multiple targets using a pulsed Doppler radar system with L electromagnetic vector sensors (EMVSs). We consider that each EMVS is composed of three electric dipoles and three magnetic loops, both are spatially colocated and orthogonal. Further, we assume that the L EMVSs are of linear nested structure. An M-level linear nested antenna array is a concatenation of M uniform linear arrays (ULAs), each of which consists of L_i antennas, with antenna spacing d_i, such that $\sum_{i=1}^{M} L_i = L$ and $d_i = \prod_{j=1}^{i-1}(L_j+1)d_1,\ i = 2, \cdots, M$. Such a geometrically simple structure is well suited for airborne application, as illustrated in Fig. 1, where the physical space available for antenna deployment is very restricted.

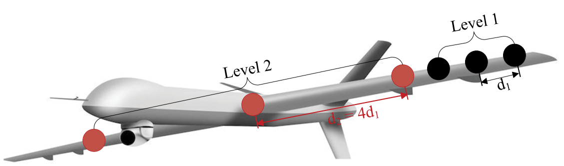

FIGURE 1. Illustration of two-level linear nested EMVSs with $L_1 = L_2 = 3$.

A. TRANSMIT SIGNAL MODEL

For a target located at angle (θ, ϕ), the EMVS produces the following 6×2 response [25]

$$\boldsymbol{Q}(\theta,\phi) = \begin{bmatrix} \cos\theta\cos\phi & -\sin\phi \\ \cos\theta\sin\phi & \cos\phi \\ -\sin\theta & 0 \\ -\sin\phi & -\cos\theta\cos\phi \\ \cos\phi & -\cos\theta\sin\phi \\ 0 & \sin\theta \end{bmatrix} \tag{1}$$

where $\theta \in [0, \pi)$ denotes the elevation angle and $\phi \in [0, 2\pi)$ represents the azimuth angle. The 2×1 baseband unit-power electrical field emitted signal can be expressed as

$$\boldsymbol{e}(t) = \boldsymbol{Q}^T(\theta,\phi)\boldsymbol{w}s(t) = \boldsymbol{\zeta}s(t) \tag{2}$$

where $\boldsymbol{w}$ is a 6×1 weights that controls the polarization of the transmit signal and $s(t)$ is the waveform of the transmit signal, $\boldsymbol{\zeta} = [\zeta_H, \zeta_V]^T$, where $\zeta_H \neq 0$ and $\zeta_V \neq 0$, respectively, represent the H- and V- components of the waveform [26]. Further, the signal transmitted in each CPI is assumed to have temporal nested structure [23], i.e., it consists of a concatenation of M uniform pulses, where each is composed of N_i pulses, with pulse interval t_i, such that $\sum_{i=1}^{M} N_i = N$ and $t_i = \prod_{j=1}^{i-1}(N_j+1)t_1,\ i = 2, \cdots, M$. Fig. 2 illustrates a two-stage nested temporal sampling with $N_1 = N_2 = 3$ for acquiring $N = 6$ pulses.

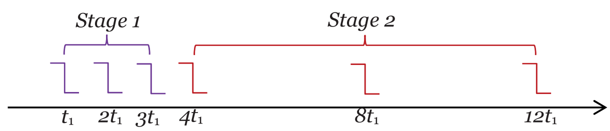

FIGURE 2. Illustration of two-stage temporal nested sampling for $N = 6$ pulses with $N_1 = N_2 = 3$ in a CPI.

B. RECEIVE SIGNAL MODEL

Consider that there are K target signals in a desired range-bin, arriving at the above described radar system. The 6×1 down-converted and match-filtered receive signal vector for the pth pulse, measured by the ℓth EMVS can be represented as

$$\begin{aligned} \boldsymbol{x}_\ell(p) &= \sum_{k=1}^{K} \rho_k(p)\boldsymbol{Q}(\theta_k,\phi_k)\boldsymbol{S}_k\boldsymbol{\zeta}a_\ell(\theta_k,\phi_k)e^{j2\pi f_k p} + \boldsymbol{n}_\ell(p) \\ &= \sum_{k=1}^{K} \rho_k(p)\boldsymbol{c}_k a_\ell(\theta_k,\phi_k)e^{j2\pi f_k p} + \boldsymbol{n}_\ell(p) \end{aligned} \tag{3}$$

where $\rho_k(p)$ is the RCS-related coefficient of the kth target at the pth pulse, $\boldsymbol{S}_k$ represents the 2×2 scattering matrix, describing the polarization transforming property of the kth target, $a_\ell(\theta_k, \phi_k) = e^{-j\frac{2\pi f_c}{c}d_\ell \sin\theta_k \cos\phi_k}$ represents the spatial response of the ℓth EMVS to the target at (θ_k, ϕ_k), in which d_ℓ denotes the position of the ℓth EMVS, and f_c is the center frequency of the band, $\boldsymbol{n}_\ell(t)$ is the additive Gaussian noise vector, which is assumed to be temporally and spatially white, with zero mean and variances σ_n^2.

In (3), $\boldsymbol{d}_k = \boldsymbol{S}_k \boldsymbol{\zeta}$ denotes the 2×1 receive polarization vector of the kth target, and $\boldsymbol{c}_k = \boldsymbol{Q}(\theta_k, \phi_k)\boldsymbol{d}_k$ is the kth target's 6×1 EMVS response vector, which has the following representation [25]

$$\boldsymbol{c}_k = \boldsymbol{Q}(\theta_k, \phi_k)\begin{bmatrix} \sin\gamma_k e^{j\eta_k} \\ \cos\gamma_k \end{bmatrix} = \begin{bmatrix} \sin\gamma_k\cos\theta_k\cos\phi_k e^{j\eta_k} - \cos\gamma_k\sin\phi_k \\ \sin\gamma_k\cos\theta_k\sin\phi_k e^{j\eta_k} + \cos\gamma_k\cos\phi_k \\ -\sin\gamma_k\sin\theta_k e^{j\eta_k} \\ -\cos\gamma_k\cos\theta_k\cos\phi_k - \sin\gamma_k\sin\phi_k e^{j\eta_k} \\ -\cos\gamma_k\cos\theta_k\sin\phi_k + \sin\gamma_k\cos\phi_k e^{j\eta_k} \\ \cos\gamma_k\sin\theta_k \end{bmatrix} \quad (4)$$

where $\gamma_k \in [0, \pi/2)$ and $\eta_k \in [-\pi, \pi)$, respectively, refer to the auxiliary polarization angle and the polarization phase difference of the kth target. Note that the above EMVS response $\boldsymbol{c}_k$ can be expressed as $\boldsymbol{c}_k = [\boldsymbol{e}_k^T, \boldsymbol{h}_k^T]$, where $\boldsymbol{e}_k$ and $\boldsymbol{h}_k$ are two 3×1 vectors, which represent, respectively, the electric field vector and the magnetic field vector.

Then, the entire $6L \times 1$ receive data vector of the EMVS array can be expressed as

$$\boldsymbol{x}(p) = \sum_{k=1}^{K}(\boldsymbol{c}_k \otimes \boldsymbol{a}_k)\rho_k(p)e^{j2\pi f_k p} + \boldsymbol{n}(p)$$

where $\boldsymbol{a}_k = \boldsymbol{a}(\theta_k, \phi_k) = [a_1(\theta_k, \phi_k), \cdots, a_L(\theta_k, \phi_k)]^T$. Furthermore, we assume that the targets are of Swerling I type, so that they are fluctuating scan-by-scan, i.e., $\rho_k(p)$ is invariant during a CPI for collection of N pulses, and fades independently from CPI to CPI. Hence, we can arrange the collected data in a CPI-by-CPI format, with the data collected in the mth CPI being expressed as

$$\begin{aligned} \boldsymbol{X}(m) &= \boldsymbol{B}\boldsymbol{P}(m)\boldsymbol{G}^T + \boldsymbol{N}(m) \\ &= (\boldsymbol{C} \odot \boldsymbol{A})\boldsymbol{P}(m)\boldsymbol{G}^T + \boldsymbol{N}(m) \end{aligned} \quad (5)$$

where $\boldsymbol{X}(m) = [\boldsymbol{x}(p_{m,1}), \boldsymbol{x}(p_{m,2}), \cdots, \boldsymbol{x}(p_{m,N})]$ is an $6L \times N$ data block, with $\boldsymbol{x}(p_{m,n}) = [\boldsymbol{x}_1(p_{m,n}), \boldsymbol{x}_2(t_{m,n}), \cdots, \boldsymbol{x}_L(p_{m,n})]^T$ being an $6L \times 1$ data vector sampled at time p_n of the mth CPI, $\boldsymbol{B} = \boldsymbol{C} \odot \boldsymbol{A} = [\boldsymbol{c}_1 \otimes \boldsymbol{a}_1, \cdots, \boldsymbol{c}_K \otimes \boldsymbol{a}_K]$ denotes the $6L \times K$ polarization-spatial response matrix, with $\boldsymbol{C} = [\boldsymbol{c}_1, \cdots, \boldsymbol{c}_k]$ and $\boldsymbol{A} = [\boldsymbol{a}_1, \cdots, \boldsymbol{a}_k]$, $\boldsymbol{G} = [\boldsymbol{g}(f_1), \cdots, \boldsymbol{g}(f_K)]$ denotes the $N \times K$ temporal response matrix, in which $\boldsymbol{g}(f_k) = [g_1(f_k), \cdots, g_N(f_k)]^T$, with $g_n(f_k) = e^{j2\pi f_k p_n}$ and p_n being the nth pulse. $\boldsymbol{N}(m) = [\boldsymbol{n}(p_{m,1}), \boldsymbol{n}(p_{m,2}), \cdots, \boldsymbol{n}(p_{m,N})]$ is the $6L \times N$ noise matrix, with $\boldsymbol{n}(p_{m,n}) = [\boldsymbol{n}_1(p_{m,n}), \boldsymbol{n}_2(p_{m,n}), \cdots, \boldsymbol{n}_L(p_{m,n})]^T$. $\boldsymbol{P}(m) = diag[\rho_1(p_m), \cdots, \rho_K(p_m)]$.

The objective of this paper is to determine the polarization, angle and frequency parameters $(\theta_k, \phi_k, \gamma_k, \eta_k, f_k)$, $k = 1, \cdots, K$ of the K targets. We provide a computationally simple solution to the above mentioned problem in Section III, under the following assumptions.

i) The angle, polarization and frequency parameters $(\theta_1, \phi_1), \cdots, (\theta_K, \phi_K)$, $f_1, \cdots, f_k$, and $(\gamma_1, \eta_1), \cdots, (\gamma_K, \eta_K)$ are pairwise distinct.
ii) The value K is known or correctly estimated.
iii) The target RCS-related coefficients $\rho_k(t)$, $k = 1, \cdots, K$ are of Rayleigh fluctuating, i.e., they are modeled as statistically independent, zero-mean complex Gaussian random processes.
iv) The noise is zero-mean, complex Gaussian, spatially uniformly white, and is statistically independent of all coefficients $\rho_k(t)$, $k = 1, \cdots, K$.

III. POLARIZATION, ANGLE AND FREQUENCY ESTIMATION

A. VIRTUAL POLARIZATION-SPATIAL-TEMPORAL MANIFOLD FORMULATION

We first divide the $6L \times N$ data block $\boldsymbol{X}(m)$ into six $L \times N$ data blocks, such that each $L \times N$ data block corresponds to a single EMVS component. Then the $L \times N$ data block $\boldsymbol{X}_i(m)$, which corresponds to the ith components of the EMVS, can be formed out of the $\boldsymbol{X}(m)$

$$\boldsymbol{X}_i(m) = \boldsymbol{A}\mathcal{D}_i(\boldsymbol{C})\boldsymbol{P}(m)\boldsymbol{G}^T + \boldsymbol{N}_i(m) \quad (6)$$

where $\mathcal{D}_i\{\cdot\}$ denotes the operator which takes the ith row of the matrix in brackets and produces a diagonal matrix by placing this row on the main diagonal. We next concatenate the columns of $\boldsymbol{X}_i(m)$ in an $LN \times 1$ vector $\boldsymbol{y}_{i,m}$ as

$$\boldsymbol{y}_{i,m} = vec\,(\boldsymbol{X}_i(m)) \quad (7)$$

Obviously, $\boldsymbol{y}_{i,m}$ has the form

$$\boldsymbol{y}_{i,m} = (\boldsymbol{G} \odot \boldsymbol{A})\mathcal{D}_i(\boldsymbol{C})\boldsymbol{\rho}(t_m) + vec(\boldsymbol{N}_i(m)) \quad (8)$$

where $\boldsymbol{\rho}(t_m) = [\rho_1(t_m), \cdots \rho_K(t_m)]^T$, $(\boldsymbol{G} \odot \boldsymbol{A})$ is the $LN \times K$ spatial-temporal manifold. For all the Q data blocks, repeating the operator (7) and arranging the obtained vectors in matrix form, we have

$$\boldsymbol{Y}_i = [\boldsymbol{y}_{i,1}, \boldsymbol{y}_{i,2}, \cdots, \boldsymbol{y}_{i,Q}] = (\boldsymbol{G} \odot \boldsymbol{A})\mathcal{D}_i(\boldsymbol{C})\boldsymbol{H} + \boldsymbol{V}_i \quad (9)$$

where $\boldsymbol{H} = [\boldsymbol{\rho}(1), \cdots, \boldsymbol{\rho}(Q)]$, $\boldsymbol{V}_i = [vec(\boldsymbol{N}_i(1)), \cdots, vec(\boldsymbol{N}_i(Q))]$. By using the assumption iii) made in Section II, the correlation matrix of $\boldsymbol{\rho}(t_m)$ has the form as

$$\boldsymbol{R}_\rho = E[\boldsymbol{\rho}(t_m)\boldsymbol{\rho}^H(t_m)] = diag(\sigma_1^2, \cdots, \sigma_K^2) \quad (10)$$

The correlation matrix between data blocks $\boldsymbol{Y}_i$ and $\boldsymbol{Y}_1$ is then given by

$$\begin{aligned} \boldsymbol{R}_i &= E[\boldsymbol{Y}_i\boldsymbol{Y}_1^H] \\ &= (\boldsymbol{G} \odot \boldsymbol{A})\mathcal{D}_i(\boldsymbol{C})\mathcal{D}_1(\boldsymbol{C}^*)\boldsymbol{R}_\rho(\boldsymbol{G} \odot \boldsymbol{A})^H + \sigma_n^2\delta_{i,1}\boldsymbol{I}_{LN} \end{aligned} \quad (11)$$

where σ_n^2 is the noise variance, and $\delta_{i,j}$ denotes the Dirac delta function. Note that the noise terms in (11) are removable by using any existing noise-estimation procedure. For convenience, we regard $\boldsymbol{R}_i$ as its noise-free counterparts hereafter. In fact, for the case where noise is taken into account, all the derivations become only approximate.

By vectorizing $\boldsymbol{R}_i$, we can get the following vector

$$\boldsymbol{r}_i = vec(\boldsymbol{R}_i) = \left[(\boldsymbol{G} \odot \boldsymbol{A})^* \odot (\boldsymbol{G} \odot \boldsymbol{A})\right]\mathcal{D}_i(\boldsymbol{C})\boldsymbol{\beta} \quad (12)$$

where $\beta = [c_{i,1}^*\sigma_1^2, \cdots, c_{i,K}^*\sigma_K^2]^T$, with $c_{i,k}$ denoting the (i,k)th entry of the matrix $\boldsymbol{C}$. Defining the following permutation matrix $\boldsymbol{P}$

$$\boldsymbol{P} = (\boldsymbol{I}_L \otimes \boldsymbol{U}_{N^2\times L})(\boldsymbol{U}_{N\times L} \otimes \boldsymbol{I}_{NL}) \tag{13}$$

where $\boldsymbol{U}_{P\times Q}$ is a a $PQ \times PQ$ matrix, defined as

$$\boldsymbol{U}_{P\times Q} = \sum_{i=1}^{P}\sum_{j=1}^{Q} \boldsymbol{E}_{ij} \otimes \boldsymbol{F}_{ji} \tag{14}$$

where $\boldsymbol{E}_{ij}$ is of size $P \times Q$, with all zeros except a 1 at the (i,j)th position, and $\boldsymbol{F}_{ji}$ is of size $Q \times P$, with all zeros except a 1 at the (j,i)th position, we can obtain [23]

$$\boldsymbol{P}\left[(\boldsymbol{G} \odot \boldsymbol{A})^* \odot (\boldsymbol{G} \odot \boldsymbol{A})\right] = \left[\left(\boldsymbol{A}^* \odot \boldsymbol{A}\right) \odot \left(\boldsymbol{G}^* \odot \boldsymbol{G}\right)\right] \tag{15}$$

Then, multiplying the matrix $\boldsymbol{P}$ to the vector $\boldsymbol{r}_i$, we can obtain the row-exchanged version of $\boldsymbol{r}_i$ as

$$\tilde{\boldsymbol{r}}_i = \boldsymbol{P}\boldsymbol{r}_i = \left[\left(\boldsymbol{A}^* \odot \boldsymbol{A}\right) \odot \left(\boldsymbol{G}^* \odot \boldsymbol{G}\right)\right] \mathcal{D}_i(\boldsymbol{C})\beta \tag{16}$$

Next, stacking $\tilde{\boldsymbol{r}}_i$ for all $i = 1, \cdots, 6$, we can get $\tilde{\boldsymbol{r}} = [\tilde{\boldsymbol{r}}_1^T, \tilde{\boldsymbol{r}}_2^T, \cdots, \tilde{\boldsymbol{r}}_6^T]^T$. It can be easily verified that $\tilde{\boldsymbol{r}}$ can be expressed via Khatri-Rao matrix product format as

$$\tilde{\boldsymbol{r}} = \left[\boldsymbol{C} \odot \left(\boldsymbol{A}^* \odot \boldsymbol{A}\right) \odot \left(\boldsymbol{G}^* \odot \boldsymbol{G}\right)\right]\beta \tag{17}$$

Obviously, the vector $\tilde{\boldsymbol{r}}$ can be considered as a new signal vector with $6(LN)^2 \times K$ manifold $\boldsymbol{C} \odot \left(\boldsymbol{A}^* \odot \boldsymbol{A}\right) \odot \left(\boldsymbol{G}^* \odot \boldsymbol{G}\right)$ and $K \times 1$ coefficient β. Moreover, $\boldsymbol{C} \odot \left(\boldsymbol{A}^* \odot \boldsymbol{A}\right) \odot \left(\boldsymbol{G}^* \odot \boldsymbol{G}\right)$ is called as virtual polarization-spatial-temporal (PST) manifold with equivalent polarization manifold $\boldsymbol{C}$, spatial manifold $(\boldsymbol{A}^* \odot \boldsymbol{A})$ and temporal manifold $(\boldsymbol{G}^* \odot \boldsymbol{G})$.

Using the difference coarray property of the two-level nested array, each column of $(\boldsymbol{A}^* \odot \boldsymbol{A})$ contains $2L_2(L_1+1)-1$ different elements. These elements can be viewed as spatial response of a $2L_2(L_1+1)-1$-element uniform linear array with antennas located from $(1-L_2(L_1+1))d_1$ to $(L_2(L_1+1)-1)d_1$. Similarly, each column of $(\boldsymbol{G}^* \odot \boldsymbol{G})$ contains $2N_2(N_1+1)-1$ different elements. These elements can be viewed as uniformly sampling of a set of monochromatic signals from time $(1-N_2(N_1+1))t_1$ to $(N_2(N_1+1)-1)t_1$. By removing the repeated items in $\boldsymbol{A}^* \odot \boldsymbol{A}$ and $\boldsymbol{G}^* \odot \boldsymbol{G}$, we can form the following vector

$$\bar{\boldsymbol{r}} = \left(\boldsymbol{C} \odot \bar{\boldsymbol{A}} \odot \bar{\boldsymbol{G}}\right)\beta \tag{18}$$

where $\bar{\boldsymbol{A}} = [\bar{\boldsymbol{a}}_1, \cdots, \bar{\boldsymbol{a}}_K]$, with $\bar{\boldsymbol{a}}_k = [e^{-j\frac{2\pi f_c}{c}(1-\bar{L})d_1\sin\theta_k}, e^{-j\frac{2\pi f_c}{c}(2-\bar{L})d_1\sin\theta_k}, \cdots, e^{-j\frac{2\pi f_c}{c}(\bar{L}-1)d_1\sin\theta_k}]^T$, is a $(2\bar{L}-1 \times K)$ Vandermonde matrix, with $\bar{L} = L_2(L_1+1)$, and $\bar{\boldsymbol{G}} = [\bar{\boldsymbol{g}}_1, \cdots, \bar{\boldsymbol{g}}_K]$, with $\bar{\boldsymbol{g}}_k = [e^{j2\pi f_k(1-\bar{N})t_1}, e^{j2\pi f_k(2-\bar{N})t_1}, \cdots, e^{j2\pi f_k(\bar{N}-1)t_1}]^T$ is a $(2\bar{N}-1 \times K)$ Vandermonde matrix, with $\bar{N} = N_2(N_1+1)$. In equation (18), $\left(\boldsymbol{C} \odot \bar{\boldsymbol{A}} \odot \bar{\boldsymbol{G}}\right)$ behaves like a PST manifold with degrees of freedom $\mathcal{O}\left(6(LN)^2\right)$. This enhanced degrees of freedom enables to offer better identifiability performance and higher parameter estimation accuracy, as will shown in the subsequent sections.

Note that for fixed L, the spatial degrees-of-freedom can be obtained is $L_2(L_1+1)$. Therefore, a criterion for dividing L into L_1 and L_2 is to choose L_1 and L_2 such that $L_2(L_1+1)$ is maximized. In this way, we choose $L_1 = L_2 = L/2$ for even L or $L_2 = L_1 + 1 = (L+1)/2$ for odd L. Analogously, $N_1 = N_2 = N/2$ is chosen for even N or $N_2 = N_1 + 1 = (N+1)/2$. for odd N.

B. DIRECT DATA AUGMENTATION FOR PARAMETER IDENTIFICATION

In order to exploit the enhanced degrees of freedom for parameter estimation from the vector $\bar{\boldsymbol{r}}$, direct data augmentation technique is adopted. To utilize the direct data augmentation, we divide the manifold matrix $\bar{\boldsymbol{A}}$ into $\bar{L}$ overlapping sub-matrices, where each is of size $\bar{L} \times K$. The ith sub-matrix of $\bar{\boldsymbol{A}}$, which is denoted as $\bar{\boldsymbol{A}}_i$, is composed of the $(\bar{L}-i+1)$th to $(2\bar{L}-i)$th rows of $\bar{\boldsymbol{A}}$. Analogously, we divide the matrix $\bar{\boldsymbol{G}}$ into $\bar{N}$ overlapping sub-matrices, where each has size $\bar{N} \times K$. The ℓth sub-matrix of $\bar{\boldsymbol{G}}$, which is denoted as $\bar{\boldsymbol{G}}_\ell$, is composed of the $(\bar{N}-\ell+1)$th to $(2\bar{N}-\ell)$th rows of $\bar{\boldsymbol{G}}$. Then, the vector $\bar{\boldsymbol{r}}_{i,\ell}$, which is associated with $\bar{\boldsymbol{A}}_i$ and $\bar{\boldsymbol{G}}_\ell$, can be extracted from $\bar{\boldsymbol{r}}$ and expressed as

$$\bar{\boldsymbol{r}}_{i,\ell} = \boldsymbol{J}_{i,\ell}\bar{\boldsymbol{r}} = \left(\boldsymbol{C} \odot \bar{\boldsymbol{A}}_i \odot \bar{\boldsymbol{G}}_\ell\right)\beta \tag{19}$$

where $\boldsymbol{J}_{i,\ell}$ is the selection matrix, defined as

$$\boldsymbol{J}_{i,\ell} = \boldsymbol{I}_6 \otimes \tilde{\boldsymbol{J}}_i \otimes \tilde{\boldsymbol{J}}_\ell \tag{20}$$

with

$$\tilde{\boldsymbol{J}}_i = [\boldsymbol{O}_{\bar{L},\bar{L}-i}, \boldsymbol{I}_{\bar{L}}, \boldsymbol{O}_{\bar{L},i-1}] \tag{21}$$
$$\tilde{\boldsymbol{J}}_\ell = [\boldsymbol{O}_{\bar{N},\bar{N}-\ell}, \boldsymbol{I}_{\bar{N}}, \boldsymbol{O}_{\bar{N},\ell-1}] \tag{22}$$

Further, for all $i = 1, \cdots, \bar{L}$ and $\ell = 1, \cdots, \bar{N}$, we can formulate a $6\bar{L}\bar{N} \times \bar{L}\bar{N}$ matrix $\bar{\boldsymbol{R}}$ as

$$\bar{\boldsymbol{R}} = [\bar{\boldsymbol{r}}_{1,1}, \bar{\boldsymbol{r}}_{1,2}, \cdots, \bar{\boldsymbol{r}}_{1,\bar{N}}, \bar{\boldsymbol{r}}_{2,1}, \cdots, \bar{\boldsymbol{r}}_{\bar{L},\bar{N}}] \tag{23}$$

We prove in the following theorem that the matrix $\bar{\boldsymbol{R}}$ can be applied to subspace-based algorithms for parameter estimation.

Theorem 1: The matrix $\bar{\boldsymbol{R}}$ defined in (23) can be expressed

$$\bar{\boldsymbol{R}} = (\boldsymbol{C} \odot \bar{\boldsymbol{A}}_1 \odot \bar{\boldsymbol{G}}_1)\bar{\boldsymbol{S}}(\bar{\boldsymbol{A}}_1 \odot \bar{\boldsymbol{G}}_1)^H \tag{24}$$

where $\bar{\boldsymbol{S}} = diag(\beta)$ is a $K \times K$ diagonal matrix.

Proof: See Appendix I.

Obviously, the matrix $\bar{\boldsymbol{R}}$ has the same structure as the data observed by PST manifold $(\boldsymbol{C} \odot \bar{\boldsymbol{A}}_1 \odot \bar{\boldsymbol{G}}_1)$ with $\bar{L}\bar{N}$ samples $\bar{\boldsymbol{S}}(\bar{\boldsymbol{A}}_1 \odot \bar{\boldsymbol{G}}_1)^H$. The matrices $\bar{\boldsymbol{A}}_1$ and $\bar{\boldsymbol{G}}_1$ are both Vandermonde matrices, and hence they are both unambiguous. Therefore, the PST manifold $(\boldsymbol{C} \odot \bar{\boldsymbol{A}}_1 \odot \bar{\boldsymbol{G}}_1)$ is unambiguous for $K \leq \bar{L}\bar{N}$. In order for an polarization-angle-frequency subspace to exist, both $(\boldsymbol{C} \odot \bar{\boldsymbol{A}}_1 \odot \bar{\boldsymbol{G}}_1)$ and $(\bar{\boldsymbol{A}}_1 \odot \bar{\boldsymbol{G}}_1)$ are required to be tall matrices, i.e., $K < \bar{L}\bar{N}$. Therefore, applying subspace-based algorithms on $\bar{\boldsymbol{R}}$ for parameter estimation, up to $\bar{L}\bar{N}-1$ source signals can be resolved.

C. COMPUTATIONALLY EFFICIENT K-R SIGNAL SUBSPACE ESTIMATION

With the above discussions, subspace-based algorithms can be applied to $\bar{\boldsymbol{R}}$ for estimating polarization, angle and frequency parameters. By using the relationship in (24) and performing singular-value decomposition (SVD) to $\bar{\boldsymbol{R}}$, we can find that the $6\bar{L}\bar{N} \times K$ K-R signal subspace matrix can be obtained by choosing K left-singular vectors, which are associated with the K largest singular values of $\bar{\boldsymbol{R}}$. Unfortunately, direct estimation of signal subspace matrix using SVD is computationally intensive, requiring approximately $\left(O(\bar{L}\bar{N})^6\right)$ multiplication operations. To alleviate the computational burden of the SVD, we present a computationally efficient signal subspace estimation method in this subsection.

Let $\boldsymbol{D} = (\boldsymbol{C} \odot \bar{\boldsymbol{A}}_1 \odot \bar{\boldsymbol{G}}_1)$ and partition $\boldsymbol{D}$ into

$$\boldsymbol{D} = [\boldsymbol{D}_1^T, \boldsymbol{D}_2^T]^T \tag{25}$$

where $\boldsymbol{D}_1$ and $\boldsymbol{D}_2$ are, respectively the first K rows and the remaining $(6\bar{L}\bar{N}-K)$ rows of $\boldsymbol{D}$. As analyzed in Section III-B, for $K \leq \bar{L}\bar{N} - 1$, the matrix $\boldsymbol{D}_1$ is of full rank and is invertible. Therefore, the K rows of $\boldsymbol{D}_1$ are linear independent and the rows of $\boldsymbol{D}_2$ can be expressed as linear combinations of these K rows. Mathematically, there exists a $K \times (6\bar{L}\bar{N} - K)$ linear operator $\boldsymbol{W}$ between $\boldsymbol{D}_1$ and $\boldsymbol{D}_2$, such that [27]

$$\boldsymbol{D}_2 = \boldsymbol{W}^H \boldsymbol{D}_1 \tag{26}$$

From (26), we can get

$$\boldsymbol{D}\boldsymbol{D}_1^{-1} = \boldsymbol{E}_s = \begin{bmatrix} \boldsymbol{I}_K \\ \boldsymbol{W}^H \end{bmatrix} \tag{27}$$

Since $\boldsymbol{D}_1^{-1}$ is nonsingular, it is easily seen that the columns of $\boldsymbol{D}$ and $\boldsymbol{E}_s$ span the same subspace, i.e., the signal subspace. Therefore, a solution for the signal subspace estimation can be obtained by estimating the linear operator $\boldsymbol{W}$.

In order to estimate the linear operator $\boldsymbol{W}$, we partition the matrix $\bar{\boldsymbol{R}}$ into

$$\bar{\boldsymbol{R}} = [\bar{\boldsymbol{R}}_1^T, \bar{\boldsymbol{R}}_2^T]^T \tag{28}$$

where $\bar{\boldsymbol{R}}_1$ and $\bar{\boldsymbol{R}}_2$ are, respectively the first K rows and the remaining $(6\bar{L}\bar{N} - K)$ rows of $\bar{\boldsymbol{R}}$. From (24) and (25), $\bar{\boldsymbol{R}}_1$ and $\bar{\boldsymbol{R}}_2$ can be expressed as

$$\bar{\boldsymbol{R}}_1 = \boldsymbol{D}_1 \bar{\boldsymbol{S}} (\bar{\boldsymbol{A}}_1 \odot \bar{\boldsymbol{G}}_1)^H \tag{29}$$

$$\bar{\boldsymbol{R}}_2 = \boldsymbol{D}_2 \bar{\boldsymbol{S}} (\bar{\boldsymbol{A}}_1 \odot \bar{\boldsymbol{G}}_1)^H \tag{30}$$

Therefore, from (26), (29) and (30), the linear operator $\boldsymbol{W}$ can be estimated as

$$\boldsymbol{W} = \boldsymbol{D}_1^{-H} \boldsymbol{D}_2^H = \left(\bar{\boldsymbol{R}}_1 \bar{\boldsymbol{R}}_1^H\right)^{-1} \bar{\boldsymbol{R}}_1 \bar{\boldsymbol{R}}_2^H \tag{31}$$

With the estimation of $\boldsymbol{W}$, we can form the estimation of signal subspace matrix $\boldsymbol{E}_s$ using (27).

D. POLARIZATION, ANGLE AND FREQUENCY ESTIMATION

In this subsection, we provide a polarization, angle and frequency estimation method based on the idea of ESPRIT algorithm [30]. Define the following two section matrices

$$\boldsymbol{J}_{g1} = \boldsymbol{I}_6 \otimes \boldsymbol{I}_{\bar{L}} \otimes [\boldsymbol{I}_{\bar{N}-1}, \boldsymbol{O}_{\bar{N}-1,1}] \tag{32}$$

$$\boldsymbol{J}_{g2} = \boldsymbol{I}_6 \otimes \boldsymbol{I}_{\bar{L}} \otimes [\boldsymbol{O}_{\bar{N}-1,1}, \boldsymbol{I}_{\bar{N}-1}] \tag{33}$$

We prove in Appendix II that

$$\boldsymbol{E}_{s1}^{\dagger} \boldsymbol{E}_{s2} = \boldsymbol{D}_1 \boldsymbol{\Phi}_t^* \boldsymbol{D}_1^{-1} \tag{34}$$

where $\boldsymbol{E}_{s1} = \boldsymbol{J}_{g1}\boldsymbol{E}_s$ and $\boldsymbol{E}_{s2} = \boldsymbol{J}_{g2}\boldsymbol{E}_s$.

Equation (34) establishes the relationship between the linear operator and the phase factors $\{e^{j2\pi f_k t_1}, k = 1, \cdots, K\}$, which constitute the diagonal elements of $\boldsymbol{\Phi}_t^*$. (34) also indicates that the diagonal matrix $\boldsymbol{\Phi}_t^*$ can be estimated from the eigenvalues of $\boldsymbol{E}_{s1}^{\dagger}\boldsymbol{E}_{s2}$ and the matrix $\boldsymbol{D}_1$ can be estimated from the eigenvectors of $\boldsymbol{E}_{s1}^{\dagger}\boldsymbol{E}_{s2}$. With the estimation of $\boldsymbol{\Phi}_t^*$, the Doppler frequencies of the targets can be easily calculated as

$$\hat{f}_k = \frac{arg\{[\boldsymbol{\Phi}_t^*]_{k,k}\}}{2\pi t_1} \tag{35}$$

where $arg\{z\}$ signifies the principal argument of the complex number z.

t Using the relationship in (27), the $6\bar{L}\bar{N} \times K$ PST manifold can be estimated as $\hat{\boldsymbol{D}} = \boldsymbol{E}_s\boldsymbol{D}_1$. This $6\bar{L}\bar{N} \times K$ PST manifold can be divided into six $\bar{L}\bar{N} \times K$ spatial-temporal (ST) manifolds such that each ST manifold corresponds to a single component of the EMVS. Denoting these six ST manifolds as $\hat{\boldsymbol{D}}_{e,1}, \hat{\boldsymbol{D}}_{e,2}, \hat{\boldsymbol{D}}_{e,3}, \hat{\boldsymbol{D}}_{h,1}, \hat{\boldsymbol{D}}_{h,2}$, and $\hat{\boldsymbol{D}}_{h,3}$, the EMVS manifold $\boldsymbol{C}$ can be estimated as

$$\hat{\boldsymbol{C}} = [\mathcal{M}(\hat{\boldsymbol{D}}_{e,1})^T, \mathcal{M}(\hat{\boldsymbol{D}}_{e,2})^T, \mathcal{M}(\hat{\boldsymbol{D}}_{e,3})^T, \mathcal{M}(\hat{\boldsymbol{D}}_{h,1})^T, \mathcal{M}(\hat{\boldsymbol{D}}_{h,2})^T, \mathcal{M}(\hat{\boldsymbol{D}}_{h,3})^T]^T \tag{36}$$

where $\mathcal{M}(\cdot)$ denotes the averaging operator that produces a row vector containing the mean value of each column of the matrix in brackets.

Referring back to $\boldsymbol{c}_k$ in (4), note that the electric field vector $\boldsymbol{e}_k$ and the magnetic field vector $\boldsymbol{h}_k$ are orthogonal to each other and to the source signal's Poynting vector $\boldsymbol{p}_k$, whose components are the three direction cosines along the three Cartesian coordinates, i.e.,

$$\boldsymbol{p}_k = \boldsymbol{e}_k \times \boldsymbol{h}_k = \begin{bmatrix} u_k \\ v_k \\ w_k \end{bmatrix} = \begin{bmatrix} \sin\theta_k \cos\theta_k \\ \sin\theta_k \sin\theta_k \\ \cos\theta_k \end{bmatrix} \tag{37}$$

With the estimation of $\hat{\boldsymbol{C}}$, the direction cosine estimates for the kth target can be obtained by computing the vector cross product between the normalized $\hat{\boldsymbol{e}}_k$ and the normalized $\hat{\boldsymbol{h}}_k$

$$\begin{bmatrix} \hat{u}_k \\ \hat{v}_k \\ \hat{w}_k \end{bmatrix} = \frac{\hat{\boldsymbol{e}}_k}{||\hat{\boldsymbol{e}}_k||} \times \frac{\hat{\boldsymbol{h}}_k}{||\hat{\boldsymbol{h}}_k||} \tag{38}$$

TABLE 1. Comparison of computational overheads and complexities of the methods.

Methods	Main computational overhead	Major computational complexity
Nested-Sampling: Linear Operator	correlation matrix $\boldsymbol{R}_i$ + linear operator $\boldsymbol{W}$	$\mathcal{O}((LN)^2Q + (\bar{L}\bar{N})^2K)$
Nested-Sampling: Eigendecomposition	correlation matrix $\boldsymbol{R}_i$ EVD of $\bar{\boldsymbol{R}}\bar{\boldsymbol{R}}^H$	$\mathcal{O}((LN)^2Q + (\bar{L}\bar{N})^3)$
Uniformly-Sampling: ESPRIT	correlation matrix $\boldsymbol{R}_i$ EVD of $\boldsymbol{R}_i$	$\mathcal{O}((LN)^2Q + (LN)^3)$
Uniformly-Sampling: Low Rank Decomposition	low rank decomposition	$\mathcal{O}(3K^3 + 2(6LQ + NQ + 6LN)K^2 + (6LQ + NQ + 6LN + 18LNQ)K)$

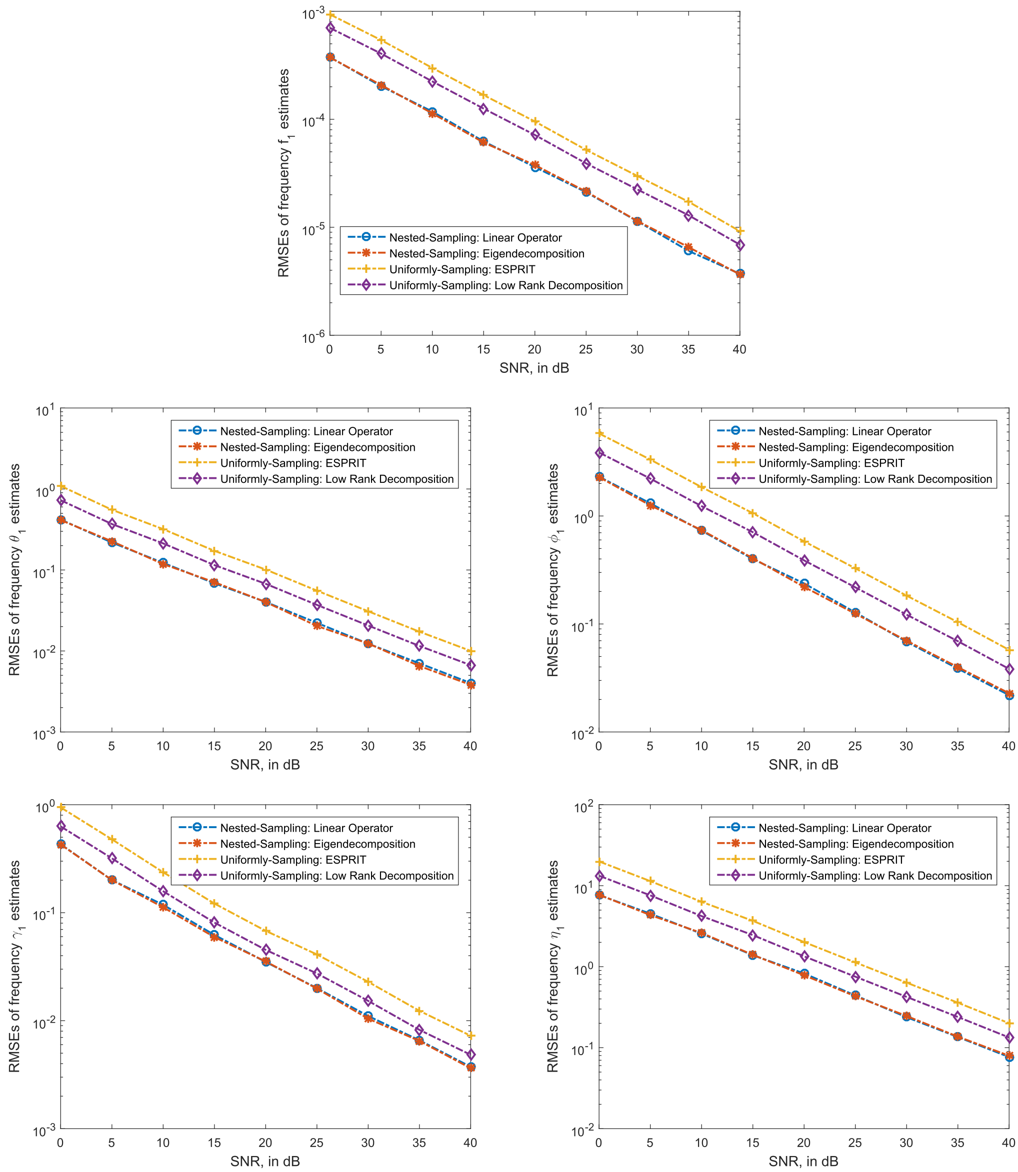

FIGURE 3. RMSE of frequency, angle and polarization estimates for the first target versus SNR. $(f_1, \theta_1, \phi_1, \gamma_1, \eta_1) = (0.1, 10^\circ, 70^\circ, 15^\circ, -90^\circ)$, and $(f_2, \theta_2, \phi_2, \gamma_2, \eta_2) = (0.2, 20^\circ, 80^\circ, 45^\circ, 90^\circ)$. $Q = 1000$, 500 independent trials are conducted.

Therefore, the azimuth, elevation and polarization parameters of the kth target can be estimated as

$$\hat{\theta}_k = \arcsin\left(\sqrt{\hat{u}_k^2 + \hat{v}_k^2}\right) \tag{39}$$

$$\hat{\phi}_k = \angle(\hat{u}_k + j\hat{v}_k) \tag{40}$$

$$\hat{\gamma}_k = \arctan|\hat{d}_{k,1}/\hat{d}_{k,2}| \tag{41}$$

$$\hat{\eta}_k = \angle d_{k,1} - \angle d_{k,2} \tag{42}$$

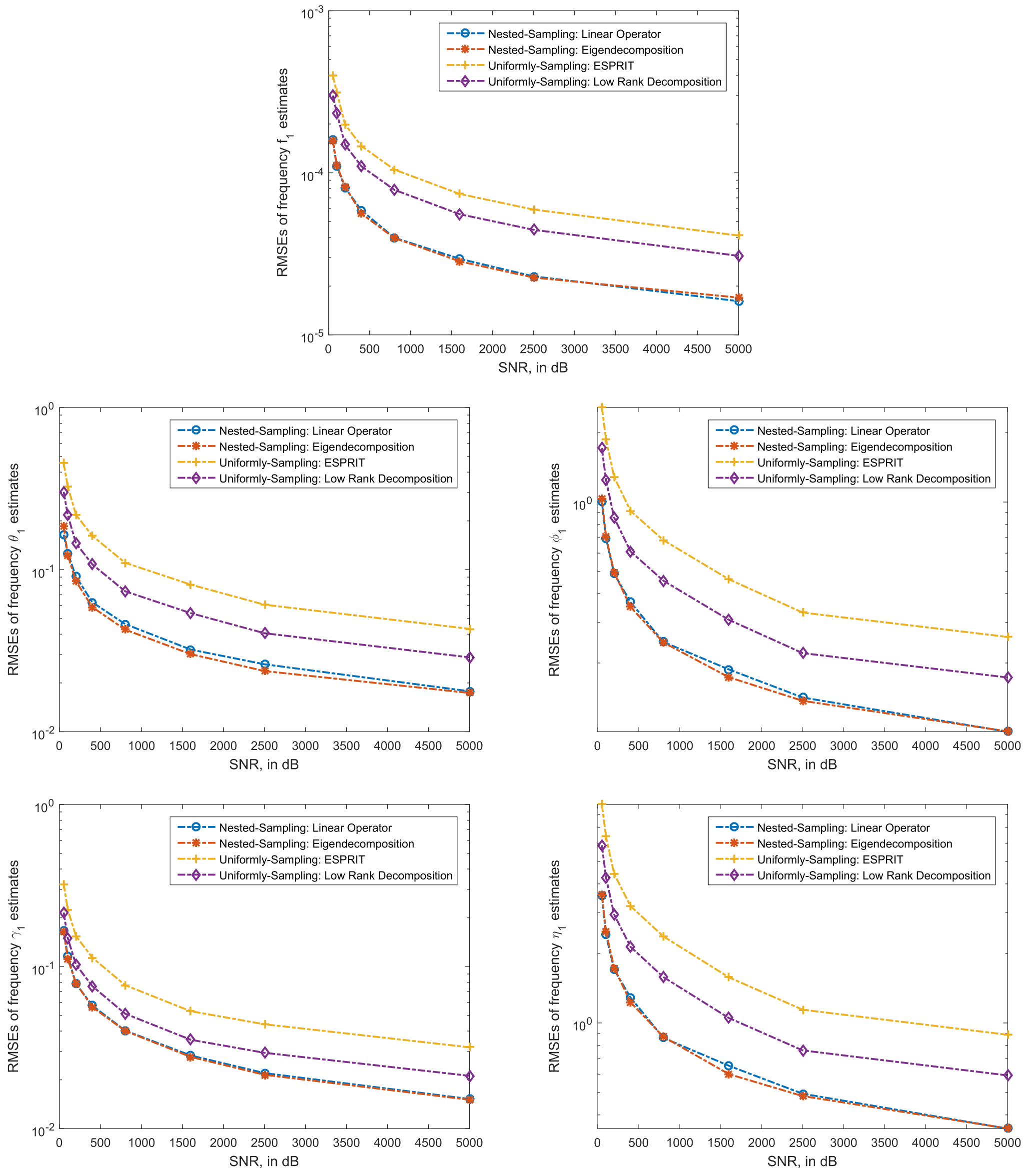

FIGURE 4. RMSE of frequency, angle and polarization estimates for the first target versus the number of CPIs. $(f_1, \theta_1, \phi_1, \gamma_1, \eta_1) = (0.1, 10°, 70°, 15°, -90°)$, and $(f_2, \theta_2, \phi_2, \gamma_2, \eta_2) = (0.2, 20°, 80°, 45°, 90°)$. SNR = 20 dB, 500 independent trials are conducted.

where

$$\hat{\boldsymbol{d}}_k = \begin{bmatrix} d_{k,1} \\ d_{k,2} \end{bmatrix} = \boldsymbol{Q}^{\dagger}(\hat{\theta}_k, \hat{\phi}_k)\hat{\boldsymbol{c}}_k \tag{43}$$

Note that the estimated angle, polarization and frequency parameters are automatically paired without any additional processing.

E. COMPUTATIONAL COMPLEXITY ANALYSIS

In this section, we analyze the computational complexities of the proposed method. Three competitive methods are considered for comparison. We use the label "Nested-Sampling: Linear Operator" for the proposed method, which uses only linear operator for signal subspace estimation. The method labeled as "Nested-Sampling: Eigendecomposition" uses eigenvalue decomposition for signal subspace estimation. The methods labeled as "Uniformly-Sampling: ESPRIT" and "Uniformly-Sampling: Low Rank Decomposition" use uniformly sampling for data acquisition, and then apply the idea of ESPRIT and low rank decomposition for parameter estimation. We consider the major computations (multiplications) involved in the methods. For the proposed method, the major computations involved are to estimate the correlation matrix $\boldsymbol{R}_i$ in (11) and to estimate the linear operator $\boldsymbol{W}$ from (31). The resulting multiplications required are in order of $\mathcal{O}((LN)^2\ Q + (\bar{L}\bar{N})^2\ K)$. For the "Nested-Sampling: Eigendecomposition" method, the major computations are to form the correlation matrix $\boldsymbol{R}_i$ and to perform the eigendecomposition of $\bar{\boldsymbol{R}}\bar{\boldsymbol{R}}^H$. The computations required

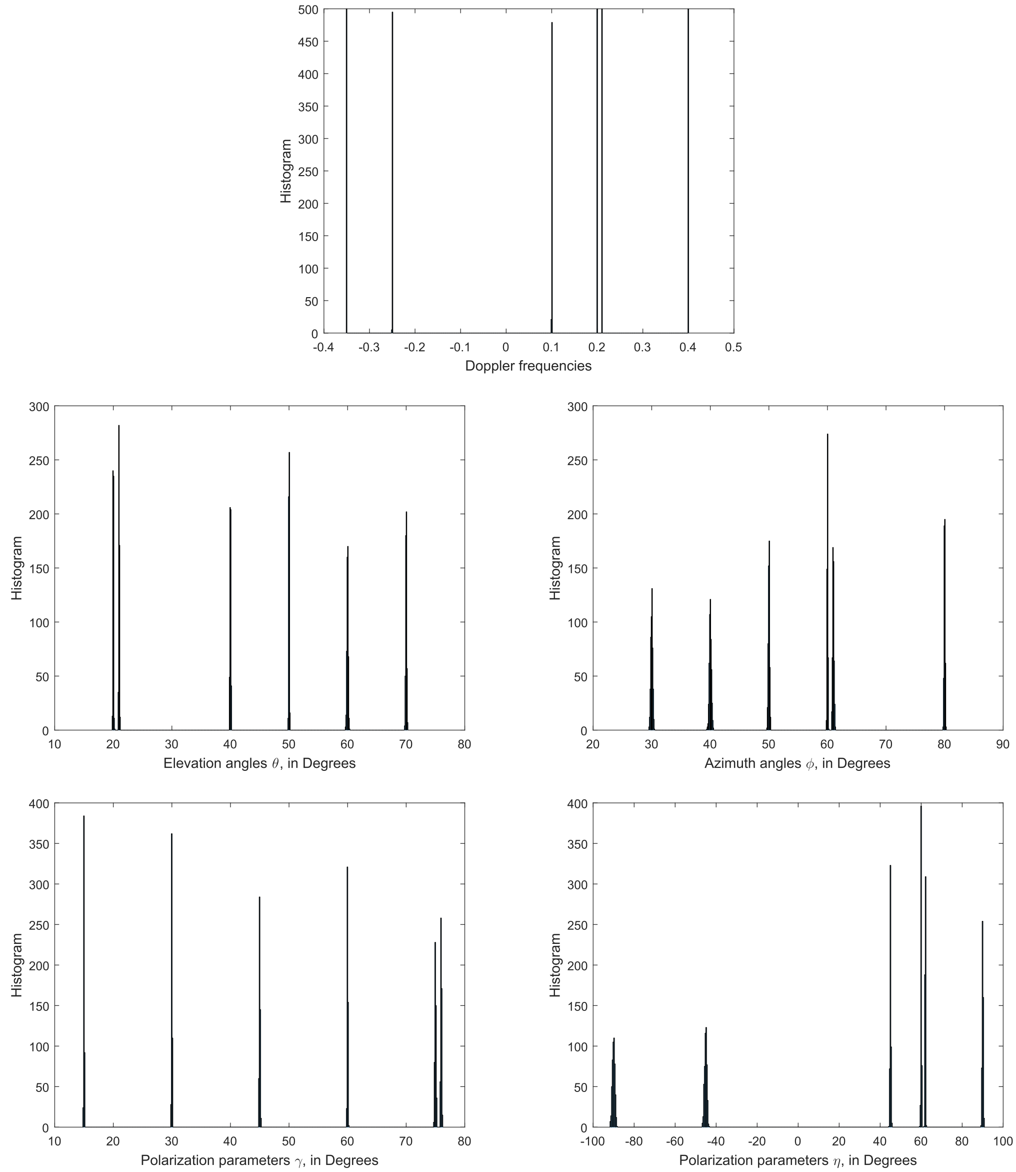

FIGURE 5. Histogram plots for the parameter estimation. $(f_1, \cdots, f_6) = (-0.35, -0.25, 0.1, 0.2, 0.3, 0.4)$, $(\theta_1, \cdots, \theta_6) = (20°, 30°, 40°, 50°, 60°, 70°)$, $(\phi_1, \cdots, \phi_6) = (30°, 40°, 50°, 60°, 70°, 80°)$, $(\gamma_1, \cdots, \gamma_6) = (5°, 15°, 30°, 45°, 60°, 75°)$, $(\eta_1, \cdots, \eta_6) = (-90°, -45°, 30°, 45°, 60°, 90°)$. *SNR* = 20 dB, *Q* = 1000, 500 independent trials are conducted.

are in order of $\mathcal{O}((LN)^2\,Q + (\bar{L}\bar{N})^3)$. For the "Uniformly-Sampling: ESPRIT" method, the major computations are to construct the matrix $\boldsymbol{R}_i$ and to perform its eigendecomposition. The multiplications needed are in order of $\mathcal{O}((LN)^2\,Q + (LN)^3)$. For the "Uniformly-Sampling: Low Rank Decomposition" method, the major computations are to perform several iterations for low rank decomposition. The multiplications involved for each iteration are in order of $\mathcal{O}(3K^3 + 2(6LQ+NQ+6LN)K^2 + (6LQ+NQ+6LN+18LNQ)K)$. For easy reference, the major computational overheads and complexities are summarized in Table 1.

IV. SIMULATION RESULTS

Simulation results are provided to compare the performance of the proposed parameter estimation method with "Nested-Sampling: Eigendecomposition", "Uniformly-Sampling: ESPRIT" and "Uniformly-Sampling: Low Rank Decomposition" methods. We consider the ESPRIT and low rank decomposition methods in that they do not require multidimensional spectral searching over parameter space and can provide closed-form solution of parameter estimates. For the nested sampling, two stage of nesting in both spatial and temporal domains are considered, with $L_1 = N_1 = 3$, $L_2 = N_2 = 2$. For uniformly sampling, a uniformly linear array with 5 antennas and 5 uniformly transmitted pulses are used. Hence, the total number of spatial-temporal data samples is the same for all the four methods. The CPI considered is $Q = 1000$ for all the methods. The additive noise is assumed to be spatial white complex Gaussian, and the signal-to-noise ratio (SNR) is defined relative to each signal.

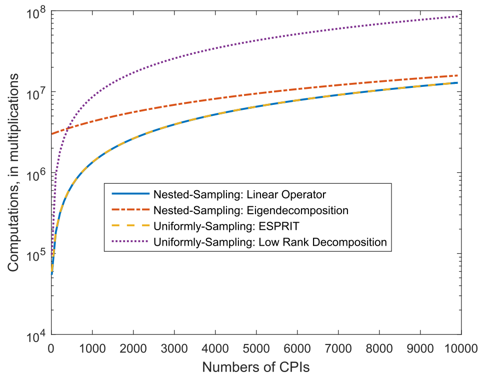

FIGURE 6. Computational costs of the methods versus the number of CPIs. $L = N = 6$, $K = 2$.

The result in each of the examples to be considered below is obtained from 500 independent Monte-Carlo trials.

In the first example, we consider a scenario of two targets with the following parameters to be estimated: $(f_1, \theta_1, \phi_1, \gamma_1, \eta_1) = (0.1, 10°, 70°, 15°, -90°)$, and $(f_2, \theta_2, \phi_2, \gamma_2, \eta_2) = (0.2, 20°, 80°, 45°, 90°)$. The Doppler frequencies are normalized with respect to the carrier frequency. Fig. 3 shows the root mean squared errors (RMSEs) of the parameter estimates of the first target as a function of SNR varying from 0 dB to 40 dB. From the figure, we see that the nested-sampling based methods have performance better than those of the uniformly-sampling based methods, in terms of lower estimation RMSEs. In addition, we can find that the performance of "Nested-Sampling: Linear Operator" and "Nested-Sampling: Eigendecomposition" are approximately the same, since their RMSE curves nearly overlap.

In the second example, we compare the performance of the methods versus the number of CPIs. The simulation conditions are the same as those in the first example, except that the SNR is fixed at 20 dB, and the number of CPIs is varied from 50 to 5000. Fig. 4 plots the RMSEs of parameter estimates of the methods. We can see from the figure that the results are similar to those shown in Fig. 3, with "Nested-Sampling: Linear Operator" and "Nested-Sampling: Eigendecomposition" exhibiting performance better than those of "Uniformly-Sampling: ESPRIT" and "Uniformly-Sampling: Low Rank Decomposition".

In the third example, we show that the proposed method is able to identify more targets than spatial or temporal samples. We assume six targets with the following parameters $(f_1, \cdots, f_6) = (-0.35, -0.25, 0.1\ 0.2, 0.21, 0.4)$, $(\theta_1, \cdots, \theta_6) = (20°, 21°, 40°, 50°, 60°, 70°)$, $(\phi_1, \cdots, \phi_6) = (30°, 40°, 50°, 60°, 61°, 80°)$, $(\gamma_1, \cdots, \gamma_6) = (5°, 15°, 30°, 45°, 74°, 75°)$, $(\eta_1, \cdots, \eta_6) = (-90°, -45°, 45°, 60°, 61°, 90°)$. The SNR is set as 20 dB. Fig. 5 shows the histogram plots for the target parameter estimation. We can observe from the figure that the proposed method can offer accurate parameter estimates when the number of targets is greater than that of the spatial or temporal samples. Incidentally, it can also work well for the cases that some of the targets have very close angle, frequency or polarization parameters.

In the last example, we compare the computational costs required by the proposed method those required by the other three methods. Fig. 6 shows the multiplications needed all the four methods as a function of the number of CPIs. The number of spatial-temporal samples are $L = N = 6$, the number target is set as $K = 2$. It is seen from the figure that the proposed method is computationally less complex than the "Nested-Sampling: Eigendecomposition" and "Uniformly-Sampling: Low Rank Decomposition". In addition, the computational costs of the proposed method and "Uniformly-Sampling: ESPRIT" are comparable.

V. CONCLUSIONS

A computationally simple joint angle, polarization and frequency estimation method for pulse doppler radar systems using a linear electromagnetic vector antenna array has been proposed in this paper. Nonuniform spatial-temporal nested sampling is used for data acquisition. RCS diversity is exploited to construct a virtual PST manifold for degrees of freedom enhancement. K-R signal subspace is estimated without performing eigenvalue decomposition. Multiple dimensional target parameters are obtained without pairing computations. Incidentally, with some computational modifications, the proposed method can also be applied to other type of EMVS array, such as dipole/loop pair and dipole/loop triads. For example, if dipole triads are used, the target angle and polarization parameters should be estimated by solving a set of nonlinear equations [11], but not from the vector cross product (38).

APPENDIX I
PROOF OF THEOREM 1

It is easily to verified that the matrices $\bar{\boldsymbol{A}}_i$ and $\bar{\boldsymbol{G}}_\ell$ are related with $\bar{\boldsymbol{A}}_1$ and $\bar{\boldsymbol{G}}_1$ as

$$\bar{\boldsymbol{A}}_i = \bar{\boldsymbol{A}}_1 \boldsymbol{\Phi}_s^{i-1} \tag{44}$$

where

$$\boldsymbol{\Phi}_s = diag\left[e^{j\frac{2\pi f_c}{c} d_1 \sin\theta_1}, \cdots, e^{j\frac{2\pi f_c}{c} d_1 \sin\theta_K}\right] \tag{45}$$

and

$$\bar{\boldsymbol{G}}_\ell = \bar{\boldsymbol{G}}_1 \boldsymbol{\Phi}_t^{\ell-1} \tag{46}$$

where

$$\boldsymbol{\Phi}_t = diag\left[e^{-j2\pi f_1 t_1}, \cdots, e^{-j2\pi f_K t_1}\right] \tag{47}$$

The vector $\bar{\boldsymbol{r}}_{i,\ell}$ can be calculated as

$$\bar{\boldsymbol{r}}_{i,\ell} = \left(\boldsymbol{C} \odot \bar{\boldsymbol{A}}_1 \odot \bar{\boldsymbol{G}}_1\right) \boldsymbol{\Phi}_s^{i-1} \boldsymbol{\Phi}_t^{\ell-1} \boldsymbol{\beta} \tag{48}$$

Since

$$\Phi_s^{i-1} \Phi_t^{\ell-1} \boldsymbol{\beta} = \bar{\boldsymbol{S}} \left(\phi_s^{i-1} \diamond \phi_t^{\ell-1}\right) \tag{49}$$

where

$$\bar{\boldsymbol{S}} = diag(\boldsymbol{\beta}) \tag{50}$$

$$\phi_s^{i-1} = \left[e^{j\frac{2\pi f_c}{c}(i-1)d_1 \sin\theta_1}, \cdots, e^{j\frac{2\pi f_c}{c}(i-1)d_1 \sin\theta_K}\right]^T \quad (51)$$

$$\phi_t^{\ell-1} = \left[e^{-j2\pi(\ell-1)f_1 t_1}, \cdots, e^{-j2\pi(\ell-1)f_K t_1}\right]^T \quad (52)$$

we have

$$\bar{\boldsymbol{R}} = \left(\boldsymbol{C} \odot \bar{\boldsymbol{A}}_1 \odot \bar{\boldsymbol{G}}_1\right) \bar{\boldsymbol{S}} \times \left[1, 1 \diamond \phi_t, 1 \diamond \phi_t^2, \cdots, \phi_s \diamond 1, \cdots, \phi_s^{\bar{L}} \diamond \phi_t^{\bar{N}}\right] \quad (53)$$

After some computations, we can obtain that

$$\left[1, 1 \diamond \phi_t, 1 \diamond \phi_t^2, \cdots, \phi_s \diamond 1, \cdots, \phi_s^{\bar{L}} \diamond \phi_t^{\bar{N}}\right] = \left(\bar{\boldsymbol{A}}_1 \odot \bar{\boldsymbol{G}}_1\right)^H \quad (54)$$

Therefore, the relationship (24) is established.

APPENDIX II
PROOF OF EQUATIONS (34)

Let $\boldsymbol{D}_{g1} = \boldsymbol{J}_{g1}\boldsymbol{D}$ and $\boldsymbol{D}_{g2} = \boldsymbol{J}_{g2}\boldsymbol{D}$, we can obtain

$$\boldsymbol{D}_{g1} = \boldsymbol{C} \odot \bar{\boldsymbol{A}}_1 \odot \bar{\boldsymbol{G}}_{1,1} \quad (55)$$

$$\boldsymbol{D}_{g2} = \boldsymbol{C} \odot \bar{\boldsymbol{A}}_1 \odot \bar{\boldsymbol{G}}_{1,2} \quad (56)$$

where $\bar{\boldsymbol{G}}_{1,1}$ and $\bar{\boldsymbol{G}}_{1,2}$ are, respectively, the first $\bar{N}-1$ and the last $\bar{N}-1$ rows of $\bar{\boldsymbol{G}}_1$. It is easily to get

$$\bar{\boldsymbol{G}}_{1,2} = \bar{\boldsymbol{G}}_{1,1}\boldsymbol{\Phi}_t^* \quad (57)$$

Therefore, we have

$$\boldsymbol{D}_{g2} = \boldsymbol{D}_{g1}\boldsymbol{\Phi}_t^* \quad (58)$$

Based on the idea of ESPRIT, we can get

$$\boldsymbol{E}_{s1} = \boldsymbol{J}_{g1}\boldsymbol{E}_s = \boldsymbol{D}_{g1}\boldsymbol{D}^{-1} \quad (59)$$

$$\boldsymbol{E}_{s2} = \boldsymbol{J}_{g2}\boldsymbol{E}_s = \boldsymbol{D}_{g2}\boldsymbol{D}^{-1} = \boldsymbol{D}_{g1}\boldsymbol{\Phi}_t^*\boldsymbol{D}^{-1} \quad (60)$$

Equations (59) and (60) together yield the relationship (34).

REFERENCES

[1] H. Chen, C. Hou, W. Liu, W.-P. Zhu, and M. N. S. Swamy, "Efficient two-dimensional direction-of-arrival estimation for a mixture of circular and noncircular sources," *IEEE Sensors J.*, vol. 16, no. 8, pp. 2527–2536, Apr. 2016.

[2] J. Liang, "Joint azimuth and elevation direction finding using cumulant," *IEEE Sensors J.*, vol. 9, no. 4, pp. 390–398, Apr. 2009.

[3] J. Li and D. Jiang, "Joint elevation and azimuth angles estimation for L-shaped array," *IEEE Antennas Wireless Propag. Lett.*, vol. 16, pp. 453–456, 2017.

[4] Z. Zhang, W. Wang, Y. Huang, and S. Liu, "Decoupled 2-D direction of arrival estimation in L-shaped array," *IEEE Commun. Lett.*, vol. 21, no. 9, pp. 1989–1992, Sep. 2017.

[5] Y.-H. Chen and C.-H. Chen, "Direction-of-arrival and frequency estimations for narrowband sources using two single rotation invariance algorithms with the marked subspace," *IEE Proc. F-Radar Signal Process.*, vol. 139, no. 4, pp. 297–300, Aug. 1992.

[6] G. Lijia, C. TianQi, and H. Xiangfu, "Simultaneous frequency and direction estimation from parallel-array data," *IEE Proc.–Radar, Sonar Navigat.*, vol. 142, no. 1, pp. 6–10, Feb. 1995.

[7] M. Djeddou, A. Belouchrani, and S. Aouada, "Maximum likelihood angle-frequency estimation in partially known correlated noise for low-elevation targets," *IEEE Trans. Signal Process.*, vol. 53, no. 8, pp. 3057–3064, Aug. 2005.

[8] X. Wang, "Joint angle and frequency estimation using multiple-delay output based on ESPRIT," *EURASIP J. Adv. Signal Process.*, vol. 2010, Dec. 2010, Art. no. 358659.

[9] X. Wang, X. Zhang, J. Li, and J. Bai, "Improved ESPRIT method for joint direction-of-arrival and frequency estimation using multiple-delay output," *Int. J. Antennas Propag.*, vol. 2012, Art. no. 309269, Jul. 2012.

[10] K. T. Wong and M. D. Zoltowski, "Uni-vector-sensor ESPRIT for multisource azimuth, elevation, and polarization estimation," *IEEE Trans. Antennas Propag.*, vol. 45, no. 10, pp. 1467–1474, Oct. 1997.

[11] J. He and Z. Liu, "Computationally efficient 2D direction finding and polarization estimation with arbitrarily spaced electromagnetic vector sensors at unknown locations using the propagator method," *Digit. Signal Process.*, vol. 19, no. 3, pp. 491–503, 2009.

[12] K. T. Wong and M. D. Zoltowski, "Closed-form direction finding and polarization estimation with arbitrarily spaced electromagnetic vector-sensors at unknown locations," *IEEE Trans. Antennas Propag.*, vol. 48, no. 5, pp. 671–681, May 2000.

[13] K. T. Wong, L. Li, and M. D. Zoltowski, "Root-MUSIC-based direction-finding and polarization estimation using diversely polarized possibly collocated antennas," *IEEE Antennas Wireless Propag. Lett.*, vol. 3, no. 8, pp. 129–132, 2004.

[14] K. Han and A. Nehorai, "Nested vector-sensor array processing via tensor modeling," *IEEE Trans. Signal Process.*, vol. 62, no. 10, pp. 2542–2553, May 2014.

[15] M. Yang, J. Ding, B. Chen, and X. Yuan, "A multiscale sparse array of spatially spread electromagnetic-vector-sensors for direction finding and polarization estimation," *IEEE Access*, vol. 6, pp. 9807–9818, Jan. 2018.

[16] P. Pal and P. P. Vaidyanathan, "Nested arrays: A novel approach to array processing with enhanced degrees of freedom," *IEEE Trans. Signal Process.*, vol. 58, no. 8, pp. 4167–4181, Aug. 2010.

[17] K. Han and A. Nehorai, "Improved source number detection and direction estimation with nested arrays and ULAs using jackknifing," *IEEE Trans. Signal Process.*, vol. 61, no. 23, pp. 6118–6128, Nov. 2013.

[18] K. Han and A. Nehorai, "Wideband Gaussian source processing using a linear nested array," *IEEE Signal Process. Lett.*, vol. 20, no. 11, pp. 1110–1113, Nov. 2013.

[19] K. Han and A. Nehorai, "Nested array processing for distributed sources," *IEEE Signal Process. Lett.*, vol. 21, no. 9, pp. 1111–1114, Sep. 2014.

[20] J. Yang, G. Liao, and J. Li, "Robust adaptive beamforming in nested array," *Signal Process.*, vol. 114, no. 6, pp. 143–149, Sep. 2015.

[21] Y.-Y. Dong, C.-X. Dong, Y.-T. Zhu, G.-Q. Zhao, and S.-Y. Liu, "Two-dimensional DOA estimation for L-shaped array with nested subarrays without pair matching," *IET Signal Process.*, vol. 10, no. 9, pp. 1112–1117, Jul. 2016.

[22] W.-Q. Wang and C. L. Zhu, "Nested array receiver with time-delayers for joint target range and angle estimation," *IET Radar, Sonar Navigat.*, vol. 10, no. 8, pp. 1384–1393, Oct. 2016.

[23] J. He, Z. H. Zhang, T. Shu, B. Tang, and W. X. Yu, "Joint DOA and frequency estimation with sub-Nyquist sampling," *IET Radar Sonar Navigat.*, vol. 11, no. 9, pp. 1373–1378, 2017.

[24] K. Wang, J. He, T. Shu, and Z. Liu, "Angle-polarization estimation for coherent sources with linear tripole sensor arrays," *Sensors*, vol. 16, no. 2, 2016, Art. no. 248.

[25] A. Nehorai and E. Paldi, "Vector-sensor array processing for electromagnetic source localization," *IEEE Trans. Signal Process.*, vol. 42, no. 2, pp. 376–398, Feb. 1994.

[26] J.-J. Xiao and A. Nehorai, "Optimal polarized beampattern synthesis using a vector antenna array," *IEEE Trans. Signal Process.*, vol. 57, no. 2, pp. 576–586, Feb. 2009.

[27] S. Marcos, A. Marsal, and M. Benidir, "The propagator method for source bearing estimation," *Signal Process.*, vol. 42, no. 2, pp. 121–138, 1995.

[28] A. N. Lemma, A.-J. van der Veen, and E. F. Deprettere, "Analysis of joint angle-frequency estimation using ESPRIT," *IEEE Trans. Signal Process.*, vol. 51, no. 5, pp. 1264–1283, May 2003.

[29] X. Liu and N. D. Sidiropoulos, "Cramer-Rao lower bounds for low-rank decomposition of multidimensional arrays," *IEEE Trans. Signal Process.*, vol. 49, no. 9, pp. 2074–2086, Sep. 2001.

[30] R. Roy and T. Kailath, "Esprit-estimation of signal parameters via rotational invariance techniques," *IEEE Trans. Acoust., Speech, Signal Process.*, vol. 37, no. 7, pp. 984–995, Jul. 1989.

XIAODONG HAN was born in Wuxi, Jiangsu, China, in 1981. He received the B.S. and M.S. degrees in electronic engineering from the Nanjing University of Science and Technology, Nanjing, China, in 2004 and 2006, respectively. He is currently pursuing the Ph.D. degree in communication and information systems with Shanghai Jiao Tong University, Shanghai, China.

Since 2006, he has been with the AVIC Leihua Electronic Technology Research Institute, where he is currently a Senior Engineer. His current research is in STAP, ground moving target indication signal processing, array signal processing, and radar system design.

TING SHU received the B.Sc. and M.Sc. degrees in electrical engineering from the Nanjing University of Science and Technology, Nanjing, China, in 2004 and 2006, respectively, and the Ph.D. degree in electrical engineering from Shanghai Jiao Tong University (SJTU), Shanghai, China, in 2010. From 2010 to 2011, he was a System Engineer with the Wireless Department, Huawei Technologies Co., Ltd., responsible for the HSDPA baseband system design for the UMTS evolution. He joined SJTU in 2011, where he is currently an Assistant Professor with the Shanghai Key Laboratory of Intelligent Sensing and Recognition. His current research interests include research and development of the hardware-in-loop simulation for radar and EW systems, real-time signal processing technique, and adaptive array for phased array radars.

JIN HE received the B.S. degree in information engineering from Tongji University, Shanghai, China, in 2001, and the M.S. and Ph.D. degrees in electrical engineering from the Nanjing University of Science and Technology (NJUST), Nanjing, Jiangsu, China, in 2004 and 2007, respectively. From 2007 to 2009, he was a Post-Doctoral Fellow with the Department of Electrical Engineering, NJUST, where he was also the Program Director and was responsible for the China Postdoctoral Science Projects. From 2009 to 2011, he was a Post-Doctoral Fellow with the Department of Electrical and Computer Engineering, Concordia University, Montreal, QC, Canada. From 2012 to 2015, he was a Research Engineer with the Shanghai Aerospace Electronic Technology Institute, Shanghai, China. He is currently an Associate Professor with the Shanghai Key Laboratory of Intelligent Sensing and Recognition, Department of Electronic Engineering, Shanghai Jiao Tong University, Shanghai. He has been serving as a peer-reviewer for various IEEE/IET research journals since 2007. His research interests include array signal processing, statistical signal processing, non-Gaussian signal processing, and their applications.

WENXIAN YU received the B.S., M.S., and Ph.D. degrees from the National University of Defense Technology, Changsha, China, in 1985, 1988, and 1993, respectively. From 1996 to 2008, he was a Professor with the College of Electronic Science and Engineering, National University of Defense Technology, where he was also the Deputy Head of the College and an Assistant Director of the National Key Laboratory of Automatic Target Recognition. From 2009 to 2011, he was the Executive Dean of the School of Electronic, Information, and Electrical Engineering, Shanghai Jiao Tong University, Shanghai, China, where he is currently a Yangtze River Scholar Distinguished Professor and the Head of the research part. His research interests include remote sensing information processing, automatic target recognition, and multisensor data fusion.